CONDENSED MATTER PHYSICS

Strongly correlated superconductivity in a copper-based metal-organic framework with a perfect kagome lattice

T. Takenaka[1]*, K. Ishihara[1]*, M. Roppongi[1], Y. Miao[1], Y. Mizukami[1], T. Makita[1], J. Tsurumi[1], S. Watanabe[1], J. Takeya[1], M. Yamashita[2], K. Torizuka[2,3], Y. Uwatoko[2], T. Sasaki[4], X. Huang[5], W. Xu[5], D. Zhu[5], N. Su[6], J.-G. Cheng[6], T. Shibauchi[1]†, K. Hashimoto[1]†

Metal-organic frameworks (MOFs), which are self-assemblies of metal ions and organic ligands, provide a tunable platform to search a new state of matter. A two-dimensional (2D) perfect kagome lattice, whose geometrical frustration is a key to realizing quantum spin liquids, has been formed in the $\pi - d$ conjugated 2D MOF $[Cu_3(C_6S_6)]_n$ (Cu-BHT). The recent discovery of its superconductivity with a critical temperature T_c of 0.25 kelvin raises fundamental questions about the nature of electron pairing. Here, we show that Cu-BHT is a strongly correlated unconventional superconductor with extremely low superfluid density. A nonexponential temperature dependence of superfluid density is observed, indicating the possible presence of superconducting gap nodes. The magnitude of superfluid density is much smaller than those in conventional superconductors and follows the Uemura's relation of strongly correlated superconductors. These results imply that the unconventional superconductivity in Cu-BHT originates from electron correlations related to spin fluctuations of kagome lattice.

INTRODUCTION

Metal-organic frameworks (MOFs), a subclass of coordination polymers with a nanoporous structure consisting of metal ions bridged by organic ligands (1), are usually insulating because of the low degree of covalency of the metal-ligand bond. Recent substantial progress in the development of electrically conductive MOFs (2–5) may open up possibilities of applications in energy storage and chemical sensing, such as batteries (6), thermoelectric devices (7), and chemiresistive sensors (8). However, most conductive MOFs are semiconducting, and thus, the realization of delocalization of electrons, that is, band transport in MOFs is highly challenging.

A promising route toward metallic MOFs is the through-bond approach, which can be achieved by improving the covalency of the metal-ligand bond (3). Under this strategy, highly conductive MOFs have been synthesized in two-dimensional (2D) layered frameworks (9–12) composed of transition metal ions, such as Ni^{2+} and Cu^{2+}, and multidentate organic ligands, such as benzenehexathiol (BHT), where the strong overlap of the d orbitals of the metal ions and the p orbitals of the organic ligand leads to delocalization of electrons with significantly higher conductivity, compared to conventional MOFs. However, in most cases, charge transport properties of such conductive 2D MOFs are dominated by thermally activated conduction, indicative of incomplete bulk metallicity due to impurities or randomness coming from grain boundaries (9–12).

Among them, copper-BHT complex with a formula of $[Cu_3(C_6S_6)]_n$ (Cu-BHT) exhibits extremely high conductivity at room temperature (~ 2500 S·cm^{-1}) (13). This material consists of stacked $\pi - d$ conjugated 2D nanosheets with Cu^{2+} ions and BHT ligands, forming a perfect kagome lattice of Cu^{2+} with $S = 1/2$ spins (see Fig. 1, A to C). In Cu-BHT, in contrast to conventional MOFs with relatively large nanopores, the Cu ions and the BHT ligands are connected in an extremely dense manner (Fig. 1A). This leads to a large hybridization of the d orbitals of the Cu ions and the π orbitals of the BHT ligands, resulting in an electronic structure having bands crossing the Fermi level, as confirmed by band structure calculations based on the lattice structure derived from x-ray diffractions (13). This unique structure of Cu-BHT and recent substantial improvement of sample quality have enabled to realize metallization in Cu-BHT, and, unexpectedly, even superconductivity at around 0.25 K has been reported (13). Note that to the best of our knowledge, this is the first report of superconductivity in coordination polymers.

The superconducting transition temperature T_c of Cu-BHT is quite low, and its pairing mechanism has been considered in the framework of the conventional weak-coupling Bardeen-Cooper-Schrieffer (BCS) theory based on electron-phonon coupling from first-principles calculations (14). However, its 2D perfect kagome lattice of $S = 1/2$ spins is a long-standing desire in material chemistry and physics to realize quantum spin liquids, and its relation with high-T_c superconductivity has been widely discussed (15–18). Recent heat capacity and magnetic susceptibility measurements in Cu-BHT (13) have revealed the absence of any long-range magnetic order down to 50 mK and the presence of strong spin fluctuations related to the kagome lattice. Strongly enhanced spin fluctuations can promote unconventional (non-BCS) superconducting pairing, which has been observed in strongly correlated electron systems, such as high-T_c cuprates, iron pnictides, organics, and heavy fermions (19–22). It is therefore quite important to experimentally determine whether the superconductivity in Cu-BHT has conventional or unconventional nature. Here, we report on a comprehensive study on the

[1]Department of Advanced Materials Science, University of Tokyo, Kashiwa, Chiba 277-8561, Japan. [2]Institute for Solid State Physics, University of Tokyo, Kashiwa, Chiba 277-8581, Japan. [3]Department of Physics, Nippon Institute of Technology, Miyashiro, Saitama 345-8501, Japan. [4]Institute for Materials Research, Tohoku University, Aoba-ku, Sendai 980-8577, Japan. [5]Beijing National Laboratory for Molecular Sciences, Key Laboratory of Organic Solids, Institute of Chemistry, Chinese Academy of Sciences, Beijing 100190, China. [6]Beijing National Laboratory for Condensed Matter Physics and Institute of Physics, Chinese Academy of Sciences, Beijing 100190, China.
*These authors contributed equally to this work.
†Corresponding author. Email: shibauchi@k.u-tokyo.ac.jp (T.Sh.); k.hashimoto@edu.k.u-tokyo.ac.jp (K.H.)
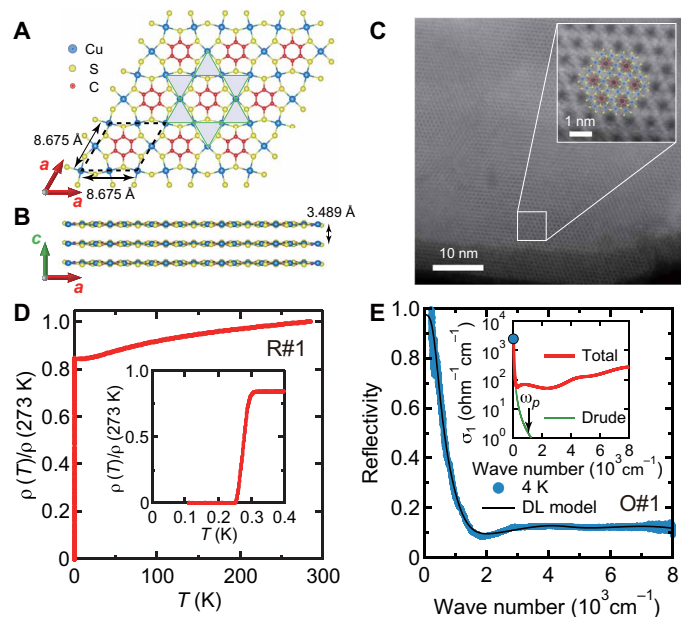
Fig. 1. Crystal structure of Cu-BHT and its transport and optical properties. (**A** and **B**) Crystal structure of Cu-BHT viewed along the c direction (A) and viewed from the side (B). The lattice parameters, a = 8.675 Å and c = 3.489 Å, were determined by the powder x-ray diffraction pattern [13]. The black dotted parallelogram in (A) indicates the in-plane unit cell. The green shaded area indicates the perfect kagome lattice of Cu^{2+} ions. (**C**) High-resolution transmission electron microscopy image of Cu-BHT. The top right inset displays the amplified image with higher magnification focused on the square area in the main panel. (**D**) Temperature dependence of the in-plane resistivity in Cu-BHT. The inset shows the low-temperature data below 0.4 K. A sharp superconducting transition is observed at around 0.25 to 0.3 K. (**E**) Optical reflectivity spectra (blue circles) in Cu-BHT measured at 4 K. The black solid line is the fit to the Drude-Lorentz (DL) model. The inset shows the optical conductivity spectra (red line) obtained from the optical reflectivity (see the Supplementary Materials). The green line represents the Drude term. The blue circle in the inset shows the value of the dc conductivity obtained from the standard four-probe method at 4 K ($\sigma_1(0) = 1/\rho = 2500$ ohm^{-1}cm^{-1}), which is consistent with $\sigma_1(0)$ obtained from the optical measurements. The plasma frequency ω_p was estimated to be ~880 cm^{-1}, at which $\sigma_1(\omega)$ of the Drude term becomes almost zero.

superconducting properties of Cu-BHT via transport, optical, and magnetic penetration depth measurements, which reveals that contrary to the theoretical proposal [14], Cu-BHT is a new member of strongly correlated unconventional superconductors, possibly originating from electron correlations enhanced by geometrical frustration of the kagome lattice.

RESULTS

Transport and optical properties of Cu-BHT

Highly crystalline samples of Cu-BHT with a thin-film structure studied here were prepared via the liquid-liquid interface reaction (see the Supplementary Materials) [11, 13]. Figure 1D shows the temperature dependence of normalized in-plane dc resistivity ρ in Cu-BHT, demonstrating a metallic behavior ($d\rho/dT > 0$) down to low temperatures, accompanied by a clear superconducting transition at around 0.25 K (see the inset of Fig. 1D). Note that we have measured multiple samples of Cu-BHT, all of which show a clear superconducting transition, but T_c is somewhat different among samples (see

fig. S1). This could be related to the unconventional superconductivity of Cu-BHT, as discussed later.

The metallic behavior in Cu-BHT has been also confirmed in optical spectroscopy measurements. Figure 1E shows the optical reflectivity spectra $R(\omega)$ of Cu-BHT. In general, in metals, the so-called Drude response can be observed in $R(\omega)$, in which two characteristic features are detected [23]; one is a high reflectivity value close to unity in the low-energy region, and the other is the plasma edge given by $\omega_p = \sqrt{e^2 n_{3D}/(\epsilon_0 m^*)}$ (where n_{3D} and m^* are the 3D carrier density and effective mass of conducting electrons, respectively), above which $R(\omega)$ starts to saturate. Both features can be clearly seen in $R(\omega)$ of Cu-BHT; as wave number approaches zero, $R(\omega)$ goes to unity, whereas $R(\omega)$ shows a saturation at around 1000 to 2000 cm^{-1} (see Fig. 1E). The overall spectra of the reflectivity can be well fitted to the Drude-Lorentz model, from which we have extracted the corresponding optical conductivity spectra $\sigma_1(\omega)$ including a Drude term, as shown in the inset of Fig. 1E (see the Supplementary Materials). These metallic features observed both in the dc limit and at finite frequencies provide strong evidence for the realization of band transport in Cu-BHT.
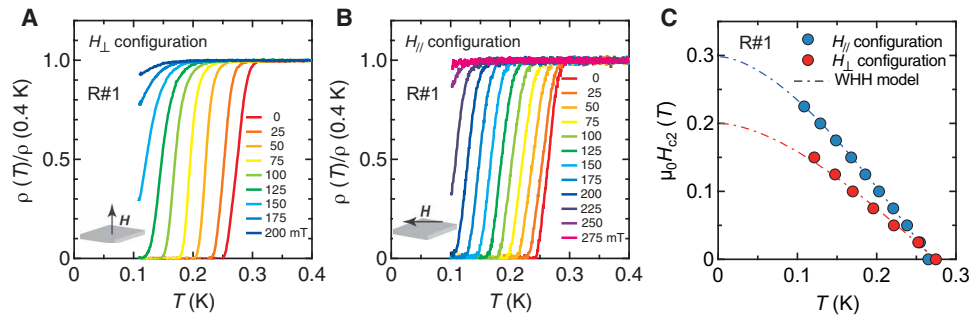
Upper critical fields of Cu-BHT

Having established that band transport is realized in Cu-BHT, we next discuss the superconducting nature of Cu-BHT. To this end, first we measured the upper critical field H_{c2}. Figure 2 (A and B) shows the temperature dependence of in-plane resistivity in magnetic fields perpendicular ($H_\perp$) and parallel ($H_\parallel$) to the in-plane direction, respectively. The superconducting state is maintained up to higher magnetic fields for the $H_\parallel$ configuration than for the $H_\perp$ configuration. Figure 2C depicts the temperature dependence of the perpendicular and parallel upper critical fields, $H_{c2\perp}(T)$ and $H_{c2\parallel}(T)$. For both directions, H_{c2} is well described by the Werthamer-Helfand-Hohenberg (WHH) model [24]. The observed anisotropy parameter $\gamma \equiv H_{c2\parallel}(0)/H_{c2\perp}(0) \sim 1.5$ is comparable to those of iron-based superconductors such as $SrFe_2(As_{1-x}P_x)_2$ [25] and LiFeAs [26] with cylindrical Fermi surfaces (γ = 1.4 and 1.3, respectively), indicating the quasi-2D nature of superconductivity in Cu-BHT. Note that the out-of-plane coherence length of Cu-BHT is estimated to be $\xi_\perp$ = 27 nm, which is much shorter than the thickness of the superconducting region of the Cu-BHT samples studied here (~2.5 μm), meaning that the quasi-2D superconductivity of Cu-BHT originates from the electronic structure itself not from the thin-film effect.

Superconducting gap structure of Cu-BHT

An important question concerning the newly found quasi-2D superconductivity in Cu-BHT is what is the interaction that glues the electrons into Cooper pairs. Conventional phonon-mediated pairing leads to a superconducting gap opening all over the Fermi surfaces, while unconventional pairing mechanisms, such as spin fluctuations, can lead to an anisotropic gap with nodes where the superconducting gap becomes zero [27]. Such a nodal structure has been observed in d-wave superconductors such as cuprates, heavy fermions, and organic conductors, where the low-energy superconducting quasiparticle excitations remain finite even at low temperatures.

There are several physical quantities sensitive to the superconducting quasiparticle excitations. Among them, magnetic penetration depth λ, which is one of the most fundamental properties of superconductors [28], is a sensitive probe of the low-energy

Fig. 2. Anisotropy of the upper critical fields of Cu-BHT. (**A** and **B**) Temperature dependence of the in-plane resistivity in magnetic fields applied perpendicular (A) and parallel (B) to the in-plane direction. (**C**) Temperature dependence of the upper critical fields for the $H_{\parallel}$ configuration (blue circles) and the $H_{\perp}$ configuration (red circles). Here, we defined $\mu_0 H_{c2}$ as a field at which the resistivity becomes 50% of the normal-state value. The dashed lines represent the WHH model (24). The anisotropy of H_{c2} is estimated to be 1.5, and the in-plane and out-of-plane coherence lengths were estimated to be $\xi_{\parallel} = 41$ nm and $\xi_{\perp} = 27$ nm, respectively, through the relations, $H_{c2\perp}(0) = \Phi_0/\left(2\pi \xi_{\parallel}^2\right)$ and $H_{c2\parallel}(0) = \Phi_0/(2\pi\xi_{\parallel}\xi_{\perp})$, where $\Phi_0 = 2.07 \times 10^{-15}$ Wb is the flux quantum.

quasi-particle excitations, and it directly relates with the 3D carrier density of superconducting electrons n_{3D} through the relation $\lambda^2(0) = m^*/(\mu_0 e^2 n_{3D})$, where $\lambda(0)$ is the magnetic penetration depth at absolute zero, and m^* is the effective mass of the superconducting carriers. In this study, we measured the magnetic penetration depth of Cu-BHT down to 40 mK by using a tunnel diode oscillator (TDO) in a dilution refrigerator (see the Supplementary Materials). Figure 3A shows the total frequency shift accompanied by the superconducting transition, which is directly related to the magnetic susceptibility χ and magnetic penetration depth λ. A clear drop in the frequency shift has been observed at 0.2 to 0.25 K, which confirms the superconducting Meissner state, evidencing bulk superconductivity in Cu-BHT. A relatively broad superconducting transition may be attributed to the thin-film structure of Cu-BHT; the magnetic penetration depth near T_c becomes longer than the thickness of the superconducting region of the sample, which prevents a full superconducting shielding, resulting in the broad superconducting transition (29). The importance of phase fluctuations in superconductors with small superfluid density has been discussed in quasi-2D superconductors (30), which may also broaden the superconducting transition. Since Cu-BHT has a 2D structure with extremely low superfluid density discussed later, the effect of phase fluctuations near T_c may affect the superconducting transition width.

Next, we focus on the low-temperature part of the magnetic penetration depth measurements. The absolute value of $\lambda(0) = \sqrt{m^*/(\mu_0 e^2 n_{3D})}$ is estimated to be $\sim$1.8 μm from the plasma frequency $\omega_p = \sqrt{e^2 n_{3D}/(\epsilon_0 m^*)} \approx 880$ cm^{-1} obtained in the optical measurements at 4 K through the relation $\lambda(0) = c/\omega_p$ (here, $c = 1/\sqrt{\epsilon_0 \mu_0}$ is the velocity of light), which is comparable to the typical thickness of the superconducting region of the present Cu-BHT samples ($\sim$2.5 μm). In general, when the thickness t of a superconductor is comparable to the magnetic penetration depth λ, we need to consider the so-called Pearl length $\Lambda_{eff} = \lambda^2/t_{eff}$ [where $t_{eff} = 2\lambda \tanh(t/2\lambda)$] as the 2D screening length (31, 32). By considering such a thin-film effect, we obtained the magnetic penetration depth from the measured frequency shift (for details, see the Supplementary Materials). Figure 3B depicts $\delta\lambda(T)/\lambda(0)$ as a function of T/T_c, where $\delta\lambda(T) \equiv \lambda(T) - \lambda(0)$. In conventional BCS superconductors with an isotropic full-gap structure, the temperature variation of the magnetic penetration depth is of an activated type at low temperatures (28), $\delta\lambda(T)/\lambda(0) \approx \sqrt{\pi\Delta_0/(2 k_B T)} \exp\left[-\Delta_0/(k_B T)\right]$ with $\Delta_0 = 1.76\, k_B T_c$. Thus, $\delta\lambda(T)/\lambda(0)$ becomes almost T independent at low temperatures. In stark

contrast, $\delta\lambda(T)/\lambda(0)$ of Cu-BHT shows a steeper slope at low temperatures (see Fig. 3B).

In unconventional superconductors with line nodes in the gap such as d-wave cuprates, the low-temperature $\delta\lambda(T)$ is proportional to T (33). There are a few mechanisms that can affect the exponent α in the power-law temperature dependence of $\delta\lambda(T) \propto T^{\alpha}$. It has been discussed that the effects of nonmagnetic impurity scattering (33) and quantum criticality (34) tend to increase the exponent α. In d-wave superconductors, the nonmagnetic impurity effect (33) changes the low-temperature variation of λ from T to T^2, whereas in quantum critical superconductors with line nodes, a $T^{1.5}$ dependence is often found, which is related to the temperature-dependent mass renormalization (34–36). Thus, the low-temperature exponent α in the line-node case is expected as $1 \leq \alpha \leq 2$. As shown in the inset of Fig. 3B, $\delta\lambda(T)/\lambda(0)$ follows a T^2 dependence. Thus, the obtained T^2 behavior is consistent with the presence of line nodes in the superconducting gap function with impurities.

Next, we consider magnetic impurity effects that can change the temperature dependence of the magnetic penetration depth. If the normal state of a superconductor is paramagnetic, the measured magnetic penetration depth $\lambda_m(T)$ is given by $\lambda_m(T) = \lambda_L(T)\sqrt{1 + \chi_N(T)}$ (37), where λ_L is the London penetration depth and $\chi_N(T) = 1 + C/(T + \theta_{CW})$ is the normal-state susceptibility (here, C is the Curie-Weiss constant and θ_{CW} is the characteristic temperature for magnetic interaction). Since $\chi_N(T)$ increases with decreasing temperature, $\lambda_L(T)$ shifts downward from the value of $\lambda_m(T)$ more largely at lower temperatures. Therefore, if the paramagnetic effect exists in Cu-BHT, $\lambda_L(T)$ shows a steeper temperature dependence than $\lambda_m(T)$ and the exponent of $\delta\lambda_L(T) \propto T^{\alpha}$ becomes smaller than that of $\delta\lambda_m(T)$. Such analysis results have been obtained in electron-doped cuprates (37, 38) and iron-based superconductors (39). Thus, even if we consider the paramagnetic effect for Cu-BHT, the exponent of $\delta\lambda_L(T) \propto T^{\alpha}$ is expected to be smaller than 2, suggesting the presence of gap nodes in Cu-BHT. We also note that in the presence of local magnetic impurities that act as free spins, conventional (s-wave) full-gap superconductivity can change to a gapless state, resulting in a T^2 dependence of $\delta\lambda(T)$ (28, 40). However, in our present experiment down to $\sim$40 mK, no Curie term due to local magnetic impurities has been observed in the frequency change of the TDO. The TDO measurements are very sensitive to the presence of local magnetic impurities, which can be detected as a low-temperature upturn in the frequency change described by the Curie law with $\theta_{CW} \sim 0$. Such an upturn in
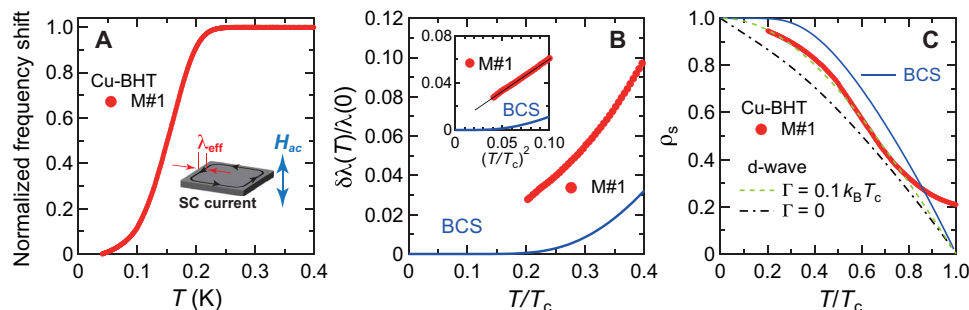
Fig. 3. Magnetic penetration depth and normalized superfluid density of Cu-BHT. (**A**) TDO frequency shift normalized by the total shift during the superconducting transition. The inset shows the schematic illustration of the superconducting screening current in an ac magnetic field. (**B**) Change in the magnetic penetration depth normalized by $\lambda(0)$ (red circles) plotted against T/T_c. The blue solid line represents the fully gapped behavior expected in the conventional s-wave (BCS) case ($\Delta_0 = 1.76\, k_B T_c$). Inset: The same data plotted against $(T/T_c)^2$. (**C**) Normalized superfluid density plotted against T/T_c. The blue solid line shows the behaviors expected in the s-wave (full gap with $\Delta_0 = 1.76\, k_B T_c$) case. The green (scattering parameter $\Gamma = 0.1\, k_B T_c$) and black ($\Gamma = 0$) lines represent the d-wave (line-node gap with $\Delta_0 = 2.14\, k_B T_c$) with and without impurities, respectively (42).

the TDO technique has been observed in iron-based superconductors with a small amount of magnetic impurities on the order of 0.1% in volume (41). Therefore, the possibility of gapless excitations due to magnetic impurities is unlikely in the present Cu-BHT case.

One may also consider that strong quantum fluctuations as discussed below can break the Cooper pairs, leading to a nonexponential behavior of $\delta\lambda(T)$ even in a full-gap superconducting state. Since the magnitude of renormalization due to quantum fluctuations increases with decreasing temperature, the lower the temperature, the greater the effect of renormalization due to quantum fluctuations on the magnetic penetration depth (36). As a result, in the case of line-node superconductors, the T-linear dependence of $\delta\lambda(T)/\lambda(0)$ changes to a $T^{1.5}$ dependence in a wide temperature range as mentioned above. Likewise, in the case of fully gapped superconductors, $\delta\lambda(T)/\lambda(0)$ is expected to show a flatter temperature dependence at low temperatures. This implies that in the full-gap case, power-law behavior due to strong quantum fluctuations cannot be expected.

The superconducting transition temperature of Cu-BHT is as low as 0.25 K, making it difficult to measure the magnetic penetration depth down to low enough temperatures to precisely determine the presence or absence of nodes in the gap. Therefore, for more detailed analysis of the superconducting gap structure, we plotted the normalized superfluid density $\rho_s(T) \equiv \lambda^2(0)/\lambda^2(T)$ as a function of T/T_c (see Fig. 3C). The overall temperature dependence of ρ_s is consistent with that expected in d-wave superconductors with impurities (42) (green dashed line), evidencing the emergence of unconventional superconductivity with sign change of the superconducting order parameter in Cu-BHT. We note that a deviation from the theory near T_c may come from the thin-film effect and/or phase fluctuations near T_c, discussed above.

DISCUSSION

To discuss the unconventional superconductivity of Cu-BHT in comparison with various superconductors, we constructed the so-called Uemura plot (an empirical relation between T_c and the effective Fermi temperature T_F, see Fig. 4), together with the results of various types of superconductors (43–47). Here, T_F is proportional to the effective 2D carrier density given by $n_{2D}/(m^*/m_0)$ for 2D systems (see the Supplementary Materials). It is widely discussed that the
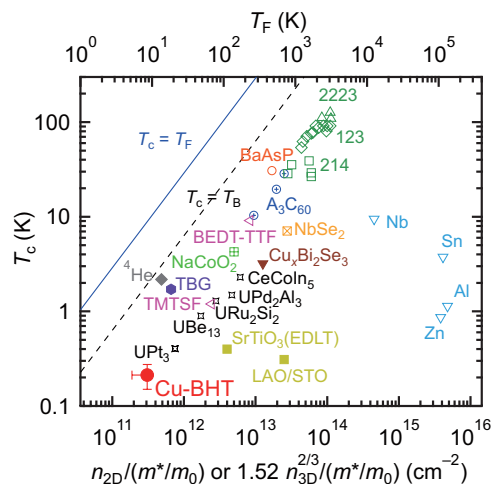
Fig. 4. Uemura plot. T_c is plotted against the effective superfluid density (bottom axis) given by $n_{2D}/(m^*/m_0)$ for 2D systems and $1.52\, n_{3D}^{2/3}/(m^*/m_0)$ for 3D systems, where n_{2D} is the carrier concentration within the superconducting planes for 2D systems, n_{3D} is the carrier concentration for 3D systems, and m_0 is the free electron mass. Here $n_{2D} = n_{3D} \times d$, where d is the interlayer spacing of the superconducting planes in 2D systems. Note that T_F (top axis) is proportional to the effective carrier density n_{2D} through the relation $T_F = \hbar^2 \pi n_{2D}/(k_B m^*)$. For Cu-BHT, the 2D formula was used (for details, see the Supplementary Materials). The error bar of T_c is determined by the sample dependence in the magnetic susceptibility measurements (see fig. S1B). The error bar of $T_F \left(= \frac{\hbar^2 \pi d}{\mu_0 e^2 k_B} \lambda^{-2}(0) \right)$ comes from the uncertainty of the absolute value of the zero-temperature magnetic penetration depth $\lambda(0)$. In this study, we evaluated $\lambda(0)$ from the plasma frequency $\omega_p = 880 \pm 80\, cm^{-1}$ measured at 4 K through the relation $\lambda(0) = c/\omega_p$. Since the previous specific heat studies (13) point to an increase in the effective mass below 1 K due to possible quantum fluctuations, the possibility that T_F decreases owing to the temperature variation of the effective mass below 1 K should be taken into account, which is the main source of the error of T_F. Therefore, we evaluated the error bar by considering that the electronic specific heat coefficient $\gamma_{el} \propto m^*$ is enhanced below 1 K from 15 mJ·mol^{-1} K^{-2} above 1 K to 40 mJ·mol^{-1} K^{-2} at 0.2 K. The black dashed line is the Bose-Einstein condensation temperature for the ideal 3D boson gas. The blue solid line represents the line where $T_c = T_F$. Here, BEDT-TTF and TMTSF stand for bis(ethylenedithio)tetrathiafulvalene and tetramethyltetraselenafulvalene, respectively, and LAO and STO represent LaAlO$_3$ and SrTiO$_3$, respectively. TBG and EDLT stand for twisted bilayer graphene and electric double layer transistor, respectively.

ratio of T_c to T_F reflects the strength of the superconducting pairing interaction; in conventional weak-coupling BCS superconductors, such as Al and Sn, T_c/T_F is quite low ($\sim 10^{-5}$), whereas in strongly correlated superconductors, such as cuprates, iron pnictides, organics, and heavy fermions, T_c/T_F becomes high ($\sim 10^{-2}$). As shown by the light blue triangles in the Uemura plot, in the conventional superconductors, only a tiny portion of electrons near the Fermi energy experience the superconducting gap, and T_c strongly varies in materials with similar superfluid densities depending on the superconducting strength. In sharp contrast, in the strongly correlated unconventional superconductors, T_c has a strong correlation with superfluid density, which is close to the linear relation expected for the Bose-Einstein condensation where the strong coupling between electrons leads to molecular-like bound pairs. What is notable here is that Cu-BHT is located on the trend line on which all the strongly correlated superconductors lie ($T_c/T_F = 0.025$ in Cu-BHT). This result implies that the unconventional superconductivity in Cu-BHT originates from strong electron correlations like other strongly correlated electron systems. We also point out that the superfluid density in this system is extremely low comparable to heavy fermion systems, corresponding to the very low $T_c \approx 0.25$ K, which places Cu-BHT on the bottom left corner in the Uemura plot.

A key question raised here is what is the mechanism of the strongly correlated unconventional superconductivity in Cu-BHT. As reported in the previous work (13), the normal-state heat capacity C and magnetic susceptibility show anomalous behaviors. The temperature dependence of C/T below 1 K follows $C/T \sim T^{-2/3}$, which is indicative of non-Fermi liquid behavior. This implies that the effective mass in the zero-temperature limit is significantly enhanced from the 4 K value, which pushes the superfluid density even smaller than that estimated from the optical spectroscopy (see the error bar in Fig. 4). Such a temperature dependence of C/T setting in at very low temperatures appears to be consistent with the extremely low effective Fermi temperature (~ 8.5 K) in this system. The Curie-Weiss analysis of the magnetic susceptibility (13) also shows an effective moment of $\mu_{eff} \sim 1.79$ μ_B close to that expected for Cu^{2+} with $S = 1/2$ spins (1.73 μ_B), with no sign of long-range magnetic ordering at least down to 2 K despite a large magnitude of the Weiss temperature of -1400 K (13). These results suggest that the present system is close to a metallic quantum spin liquid state with strong quantum fluctuations arising from the geometrically frustrated kagome-lattice structure, as discussed in geometrically frustrated Kondo lattice systems (48, 49). Recent theoretical calculations (50) have predicted the coexistence of frustrated local spins of Cu^{2+} and itinerant electrons of π orbitals in 2D MOF materials. Therefore, the unconventional pairing mechanism related to spin fluctuations in a metallic spin liquid state may be relevant in Cu-BHT. Our present findings may motivate experimental and theoretical studies on the relationship between unconventional superconductivity and quantum spin liquids. Considering the flexibility of designing crystal structures in MOFs, MOFs can provide a promising platform to study physical phenomena in condensed matter physics (51–55).

MATERIALS AND METHODS
Sample preparation
Highly crystalline samples of Cu-BHT were synthesized by the liquid-liquid interface reaction between BHT/chloroform and copper(II) nitrate/H_2O, as described in (13). The typical lateral size of the samples is larger than 1×1 mm^2, while the thickness is as small as a few micrometers. Cu-BHT films for the magnetic penetration depth measurements were cut into small pieces of samples with dimensions of about 350 μm by 350 μm.

Electrical transport measurements
The in-plane electrical resistivity was measured by the standard four-probe method in a dilution refrigerator down to 100 mK. The electrical contacts were made on the surface using carbon paste. The applied current was reduced to less than 500 nA to avoid Joule heating.

Optical reflectivity measurements
The optical reflectivity measurements were carried out with a Fourier transform microscope spectrometer in the range of 200 to 8000 cm^{-1}. In the far-infrared region (200 to 600 cm^{-1}), a synchrotron radiation light source at BL43IR in SPring-8 was used. The optical conductivity was obtained by fitting the optical reflectivity to the Drude-Lorentz model (56). The absolute value of the reflectivity was determined by comparison with a gold thin film evaporated on a glass plate, which was attached on the sample holder where the samples were fixed.

Magnetic penetration depth measurements
The temperature variation of the in-plane magnetic penetration depth $\delta\lambda(T)$ was measured by using the TDO technique operating at a resonant frequency of ~ 14 MHz in a dilution refrigerator down to ~ 40 mK (46). The sample was mounted on a sapphire rod with Apiezon N grease and inserted into a copper coil that is a part of the LC circuit. The shift in the resonant frequency δf directly reflects the change in the magnetic penetration depth $\delta\lambda$. The samples were cooled slowly (with a rate less than 1.0 K/min) to avoid introducing cracks into samples.

REFERENCES AND NOTES
1. O. M. Yaghi, M. O'Keeffe, N. W. Ockwig, H. K. Chae, M. Eddaoudi, J. Kim, Reticular synthesis and the design of new materials. *Nature* **423**, 705–714 (2003).
2. A. A. Talin, A. Centrone, A. C. Ford, M. E. Foster, V. Stavila, P. Haney, R. A. Kinney, V. Szalai, F. el Gabaly, H. P. Yoon, F. Léonard, M. D. Allendorf, Tunable electrical conductivity in metal-organic framework thin-film devices. *Science* **343**, 66–69 (2014).
3. L. Sun, S. G. Campbell, M. Dincă, Electrically conductive porous metal-organic frameworks. *Angew. Chem. Int. Ed.* **55**, 3566–3579 (2016).
4. M. Ko, L. Mendecki, K. A. Mirica, Conductive two-dimensional metal-organic frameworks as multifunctional materials. *Chem. Commun.* **54**, 7873–7891 (2018).
5. G. Skorupskii, B. A. Trump, T. W. Kasel, C. M. Brown, C. H. Hendon, M. Dincă, Efficient and tunable one-dimensional charge transport in layered lanthanide metal-organic frameworks. *Nat. Chem.* **12**, 131–136 (2020).
6. K. Wada, K. Sakaushi, S. Sasaki, H. Nishihara, Multielectron-transfer-based rechargeable energy storage of two-dimensional coordination frameworks with non-innocent ligands. *Angew. Chem. Int. Ed.* **57**, 8886–8890 (2018).
7. K. J. Erickson, F. Léonard, V. Stavila, M. E. Foster, C. D. Spataru, R. E. Jones, B. M. Foley, P. E. Hopkins, M. D. Allendorf, A. A. Talin, Thin film thermoelectric metal-organic framework with high Seebeck coefficient and low thermal conductivity. *Adv. Mater.* **27**, 3453–3459 (2015).
8. M. G. Campbell, D. Sheberla, S. F. Liu, T. M. Swager, M. Dincă, Cu_3(hexaiminotriphenylene)$_2$: An electrically conductive 2D metal-organic framework for chemiresistive sensing. *Angew. Chem.Int. Ed.* **54**, 4349–4352 (2015).

9. T. Kambe, R. Sakamoto, K. Hoshiko, K. Takada, M. Miyachi, J.-H. Ryu, S. Sasaki, J. Kim, K. Nakazato, M. Takata, H. Nishihara, π-Conjugated nickel bis(dithiolene) complex nanosheet. *J. Am. Chem. Soc.* **135**, 2462–2465 (2013).

10. T. Kambe, R. Sakamoto, T. Kusamoto, T. Pal, N. Fukui, K. Hoshiko, T. Shimojima, Z. Wang, T. Hirahara, K. Ishizaka, S. Hasegawa, F. Liu, H. Nishihara, Redox control and high conductivity of nickel bis(dithiolene) complex π-nanosheet: A potential organic two-dimensional topological insulator. *J. Am. Chem. Soc.* **136**, 14357–14360 (2014).

11. X. Huang, P. Sheng, Z. Tu, F. Zhang, J. Wang, H. Geng, Y. Zou, C. A. di, Y. Yi, Y. Sun, W. Xu, D. Zhu, A two-dimensional π − d conjugated coordination polymer with extremely high electrical conductivity and ambipolar transport behaviour. *Nat. Commun.* **6**, 7408 (2015).

12. J.-H. Dou, L. Sun, Y. Ge, W. Li, C. H. Hendon, J. Li, S. Gul, J. Yano, E. A. Stach, M. Dincă, Signature of metallic behavior in the metal-organic frameworks M_3(hexaiminobenzene)$_2$ (M = Ni, Cu). *J. Am. Chem. Soc.* **139**, 13608–13611 (2017).

13. X. Huang, S. Zhang, L. Liu, G. Chen, W. Xu, D. Zhu, Superconductivity in a copper(II)-based coordination polymer with perfect kagome structure. *Angew. Chem. Int. Ed.* **57**, 146–150 (2018).

14. X. Zhang, Y. Zhou, B. Cui, M. Zhao, F. Liu, Theoretical discovery of a superconducting two-dimensional metal-organic framework. *Nano Lett.* **17**, 6166–6170 (2017).

15. P. W. Anderson, Resonating valence bonds: A new kind of insulator? *Mater. Res. Bull.* **8**, 153–160 (1973).

16. P. W. Anderson, The resonating valence bond state in La$_2$CuO$_4$ and superconductivity. *Science* **235**, 1196–1198 (1987).

17. L. Balents, Spin liquids in frustrated magnets. *Nature* **464**, 199–208 (2010).

18. L. Savary, L. Balents, Quantum spin liquids: A review. *Rep. Prog. Phys.* **80**, 016502 (2016).

19. B. Keimer, S. A. Kivelson, M. R. Norman, S. Uchida, J. Zaanen, From quantum matter to high-temperature superconductivity in copper oxides. *Nature* **518**, 179–186 (2015).

20. Q. Si, R. Yu, E. Abrahams, High-temperature superconductivity in iron pnictides and chalcogenides. *Nat. Rev. Mater.* **1**, 16017 (2016).

21. B. J. Powell, R. H. McKenzie, Quantum frustration in organic Mott insulators: From spin liquids to unconventional superconductors. *Rep. Prog. Phys.* **74**, 056501 (2011).

22. P. Gegenwart, Q. Si, F. Steglich, Quantum criticality in heavy-fermion metals. *Nat. Phys.* **4**, 186–197 (2008).

23. M. Dressel, G. Grüner, *Electrodynamics of Solids* (Cambridge Univ. Press, 2010).

24. N. R. Werthamer, E. Helfand, P. C. Hohenberg, Temperature and purity dependence of the superconducting critical field, H_{c2}. III. Electron spin and spin-orbit effects. *Phys. Rev.* **147**, 295–302 (1966).

25. S. Yeninas, M. A. Tanatar, J. Murphy, C. P. Strehlow, O. E. Ayala-Valenzuela, R. D. McDonald, U. Welp, W. K. Kwok, T. Kobayashi, S. Miyasaka, S. Tajima, R. Prozorov, Upper critical field of isoelectron substituted SrFe$_2$(As$_{1−x}$P$_x$)$_2$. *Phys. Rev. B* **87**, 094503 (2013).

26. S. Khim, B. Lee, J. W. Kim, E. S. Choi, G. R. Stewart, K. H. Kim, Pauli-limiting effects in the upper critical fields of a clean LiFeAs single crystal. *Phys. Rev. B* **84**, 104502 (2011).

27. M. Sigrist, K. Ueda, Phenomenological theory of unconventional superconductivity. *Rev. Mod. Phys.* **63**, 239–311 (1991).

28. R. Prozorov, R. W. Giannetta, Magnetic penetration depth in unconventional superconductors. *Supercond. Sci. Technol.* **19**, R41–R67 (2006).

29. H. Kim, K. Wang, Y. Nakajima, R. Hu, S. Ziemak, P. Syers, L. Wang, H. Hodovanets, J. D. Denlinger, P. M. R. Brydon, D. F. Agterberg, M. A. Tanatar, R. Prozorov, J. Paglione, Beyond triplet: Unconventional superconductivity in a spin-3/2 topological semimetal. *Sci. Adv.* **4**, eaao4513 (2018).

30. V. J. Emery, S. A. Kivelson, Importance of phase fluctuations in superconductors with small superfluid density. *Nature* **374**, 434–437 (1995).

31. J. Pearl, Current distribution in superconducting films carrying quantized fluxoids. *Appl. Phys. Lett.* **5**, 65–66 (1964).

32. D.-X. Chen, C. Navau, N. Del-Valle, A. Sanchez, Determination of London penetration depth from ac susceptibility measurements of a square superconducting thin film. *Physica C* **500**, 9–13 (2014).

33. P. J. Hirschfeld, N. Goldenfeld, Effect of strong scattering on the low-temperature penetration depth of a d-wave superconductor. *Phys. Rev. B* **48**, 4219–4222 (1993).

34. K. Hashimoto, Y. Mizukami, R. Katsumata, H. Shishido, M. Yamashita, H. Ikeda, Y. Matsuda, J. A. Schlueter, J. D. Fletcher, A. Carrington, D. Gnida, D. Kaczorowski, T. Shibauchi, Anomalous superfluid density in quantum critical superconductors. *Proc. Natl. Acad. Sci. U.S.A.* **110**, 3293–3297 (2013).

35. Y. Mizukami, Y. Kawamoto, Y. Shimoyama, S. Kurata, H. Ikeda, T. Wolf, D. A. Zocco, K. Grube, H. v. Löhneysen, Y. Matsuda, T. Shibauchi, Evolution of quasiparticle excitations with enhanced electron correlations in superconducting AFe$_2$As$_2$ (A = K, Rb, and Cs). *Phys. Rev. B* **94**, 024508 (2016).

36. T. Nomoto, H. Ikeda, Effect of magnetic criticality and Fermi-surface topology on the magnetic penetration depth. *Phys. Rev. Lett.* **111**, 167001 (2013).

37. J. R. Cooper, Power-law dependence of the ab-plane penetration depth in Nd$_{1.85}$Ce$_{0.15}$CuO$_{4−y}$. *Phys. Rev. B* **54**, 3753–R3755 (1996).

38. R. Prozorov, R. W. Giannetta, P. Fournier, R. L. Greene, Evidence for nodal quasiparticles in electron-doped cuprates from penetration depth measurements. *Phys. Rev. Lett.* **85**, 3700–3703 (2000).

39. L. Malone, J. D. Fletcher, A. Serafin, A. Carrington, N. D. Zhigadlo, Z. Bukowski, S. Katrych, J. Karpinski, Magnetic penetration depth of single-crystalline SmFeAsO$_{1−x}$F$_x$. *Phys. Rev. B* **79**, 140501 (2009).

40. S. Skalski, O. Betbeder-Matibet, P. R. Weiss, Properties of superconducting alloys containing paramagnetic impurities. *Phys. Rev.* **136**, A1500–A1518 (1964).

41. K. Hashimoto, M. Yamashita, S. Kasahara, Y. Senshu, N. Nakata, S. Tonegawa, K. Ikada, A. Serafin, A. Carrington, T. Terashima, H. Ikeda, T. Shibauchi, Y. Matsuda, Line nodes in the energy gap of superconducting BaFe$_2$(As1$_{−x}$P$_x$)$_2$ single crystals as seen via penetration depth and thermal conductivity. *Phys. Rev. B* **81**, 220501 (2010).

42. Y. Sun, K. Maki, Impurity effects in d-wave superconductors. *Phys. Rev. B* **51**, 6059–6063 (1995).

43. Y. J. Uemura, G. M. Luke, B. J. Sternlieb, J. H. Brewer, J. F. Carolan, W. N. Hardy, R. Kadono, J. R. Kempton, R. F. Kiefl, S. R. Kreitzman, P. Mulhern, T. M. Riseman, D. L. Williams, B. X. Yang, S. Uchida, H. Takagi, J. Gopalakrishnan, A. W. Sleight, M. A. Subramanian, C. L. Chien, M. Z. Cieplak, G. Xiao, V. Y. Lee, B. W. Statt, C. E. Stronach, W. J. Kossler, X. H. Yu, Universal correlations between T_c and n_s/m^* (carrier density over effective mass) in high-T_c cuprate superconductors. *Phys. Rev. Lett.* **62**, 2317–2320 (1989).

44. Y. J. Uemura, L. P. le, G. M. Luke, B. J. Sternlieb, W. D. Wu, J. H. Brewer, T. M. Riseman, C. L. Seaman, M. B. Maple, M. Ishikawa, D. G. Hinks, J. D. Jorgensen, G. Saito, H. Yamochi, Basic similarities among cuprate, bismuthate, organic, Chevrel-phase, and heavy-fermion superconductors shown by penetration-depth measurements. *Phys. Rev. Lett.* **66**, 2665–2668 (1991).

45. Y. J. Uemura, Condensation, excitation, pairing, and superfluid density in high-T_c superconductors: The magnetic resonance mode as a roton analogue and a possible spin-mediated pairing. *J. Phys. Condens. Matter* **16**, S4515–S4540 (2004).

46. K. Hashimoto, K. Cho, T. Shibauchi, S. Kasahara, Y. Mizukami, R. Katsumata, Y. Tsuruhara, T. Terashima, H. Ikeda, M. A. Tanatar, H. Kitano, N. Salovich, R. W. Giannetta, P. Walmsley, A. Carrington, R. Prozorov, Y. Matsuda, A sharp peak of the zero-temperature penetration depth at optimal composition in BaFe$_2$(As$_{1−x}$P$_x$)$_2$. *Science* **336**, 1554–1557 (2012).

47. Y. Cao, V. Fatemi, S. Fang, K. Watanabe, T. Taniguchi, E. Kaxiras, P. Jarillo-Herrero, Unconventional superconductivity in magic-angle graphene superlattices. *Nature* **556**, 43–50 (2018).

48. S. Nakatsuji, Y. Machida, Y. Maeno, T. Tayama, T. Sakakibara, J. van Duijn, L. Balicas, J. N. Millican, R. T. Macaluso, J. Y. Chan, Metallic spin-liquid behavior of the geometrically frustrated Kondo lattice Pr$_2$Ir$_2$O$_7$. *Phys. Rev. Lett.* **96**, 087204 (2006).

49. Y. Tokiwa, J. J. Ishikawa, S. Nakatsuji, P. Gegenwart, Quantum criticality in a metallic spin liquid. *Nat. Mater.* **13**, 356–359 (2014).

50. W. Jiang, Z. Liu, J.-W. Mei, B. Cui, F. Liu, Dichotomy between frustrated local spins and conjugated electrons in a two-dimensional metal-organic framework. *Nanoscale* **11**, 955–961 (2019).

51. M. G. Yamada, T. Soejima, N. Tsuji, D. Hirai, M. Dincă, H. Aoki, First-principles design of a half-filled flat band of the kagome lattice in two-dimensional metal-organic frameworks. *Phys. Rev. B* **94**, 081102 (2016).

52. L. Dong, Y. Kim, D. Er, A. M. Rappe, V. B. Shenoy, Two-dimensional π-conjugated covalent-organic frameworks as quantum anomalous Hall topological insulators. *Phys. Rev. Lett.* **116**, 096601 (2016).

53. W. Li, L. Sun, J. Qi, P. J. Herrero, M. Dincă, J. Li, High temperature ferromagnetism in π-conjugated two-dimensional metal-organic frameworks. *Chem. Sci.* **8**, 2859–2867 (2017).

54. M. G. Yamada, H. Fujita, M. Oshikawa, Designing Kitaev spin liquids in metal-organic frameworks. *Phys. Rev. Lett.* **119**, 057202 (2017).

55. M. G. Yamada, V. Dwivedi, M. Hermanns, Crystalline Kitaev spin liquids. *Phys. Rev. B* **96**, 155107 (2017).

56. A. B. Kuzmenko, Kramers-Kronig constrained variational analysis of optical spectra. *Rev. Sci. Instrum.* **79**, 083108 (2005).

57. R. Prozorov, R. W. Giannetta, A. Carrington, F. M. Araujo-Moreira, Meissner-London state in superconductors of rectangular cross section in a perpendicular magnetic field. *Phys. Rev. B* **62**, 115–118 (2000).

58. M. Tinkham, *Introduction to Superconductivity* (McGraw-Hill, 1996).

59. D.-X. Chen, C. Navau, N. Del-Valle, A. Sanchez, Perpendicular critical-state susceptibility of square superconducting films. *Appl. Phys. Lett.* **92**, 202503 (2008).

Science Advances

Strongly correlated superconductivity in a copper-based metal-organic framework with a perfect kagome lattice

T. Takenaka, K. Ishihara, M. Roppongi, Y. Miao, Y. Mizukami, T. Makita, J. Tsurumi, S. Watanabe, J. Takeya, M. Yamashita, K. Torizuka, Y. Uwatoko, T. Sasaki, X. Huang, W. Xu, D. Zhu, N. Su, J.-G. Cheng, T. Shibauchi and K. Hashimoto

ARTICLE TOOLS	http://advances.sciencemag.org/content/7/12/eabf3996
SUPPLEMENTARY MATERIALS	http://advances.sciencemag.org/content/suppl/2021/03/15/7.12.eabf3996.DC1
REFERENCES	This article cites 57 articles, 5 of which you can access for free http://advances.sciencemag.org/content/7/12/eabf3996#BIBL
PERMISSIONS	http://www.sciencemag.org/help/reprints-and-permissions

Use of this article is subject to the Terms of Service